Materials Research Letters

ISSN: (Print) (Online) Journal homepage: https://www.tandfonline.com/loi/tmrl20

Achieving ultra-strong Magnesium–lithium alloys by low-strain rotary swaging

Yue Yang, Xiang Chen, Jinfeng Nie, Kang Wei, Qingzhong Mao, Fenghua Lu & Yonghao Zhao

To cite this article: Yue Yang, Xiang Chen, Jinfeng Nie, Kang Wei, Qingzhong Mao, Fenghua Lu & Yonghao Zhao (2021) Achieving ultra-strong Magnesium–lithium alloys by low-strain rotary swaging, Materials Research Letters, 9:6, 255-262, DOI: 10.1080/21663831.2021.1891150

To link to this article: https://doi.org/10.1080/21663831.2021.1891150

MATER. RES. LETT.
2021, VOL. 9, NO. 6, 255–262
https://doi.org/10.1080/21663831.2021.1891150

MATERIALS RESEARCH LETTERS
Taylor & Francis
Taylor & Francis Group

ORIGINAL REPORT

Achieving ultra-strong Magnesium–lithium alloys by low-strain rotary swaging

Yue Yang, Xiang Chen, Jinfeng Nie, Kang Wei, Qingzhong Mao, Fenghua Lu and Yonghao Zhao

Nano and Heterogeneous Materials Centre, School of Materials Science and Engineering, Nanjing University of Science and Technology, Nanjing, People's Republic of China

ABSTRACT

Severe plastic deformation (SPD) with deformation strain significantly larger than one is effective to strengthen metals and alloys. However, such a method will not work for Mg alloys due to their low deformability. In view of this problem, we propose a new alloy strengthening scheme of low-strain deformation, which is to introduce massive twins and stacking faults in coarse grain interior by rotary swaging (RS) at room temperature. By using this scheme, we successfully prepared an ultra-light bulk Mg-Li alloy with new strength record.

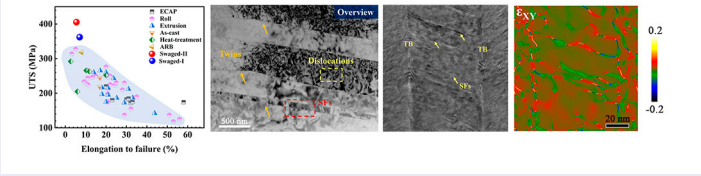

ARTICLE HISTORY
Received 19 November 2020

KEYWORDS
Mg-Li alloy; twins; stacking faults; strength

IMPACT STATEMENT

This paper explored a new strengthening way of low deformation strain for metals and alloys and successfully prepared a strongest ultra-light Mg–Li alloy by low-strain rotary swaging process.

1. Introduction

Magnesium–lithium (Mg–Li) alloys are becoming increasingly attractive as candidate metals for structural applications in the fields of aerospace, electronics and military owing to its inviting properties, such as ultra-low density, excellent formability, good damping ability and recyclability [1]. The addition of the lightest Li element not only reduces their density ($\rho \sim 1.35$–$1.65\ g/cm^3$) but also markedly improves their formability by activating $< c + a >$ pyramidal slip or modifying the crystal structure from hexagonal close packed (HCP) α-Mg phase to body centred cubic (BCC) β-Li phase with more active slip systems [2]. Although Mg–Li alloys are the lightest metallic structural materials, the phase transition with the increasing Li content leads to low mechanical strength, basically below 250 MPa [3], thereby inhibiting their widespread industrial applications.

To overcome this drawback, many routes have been proposed to strengthen Mg-Li alloys including severe plastic deformation (SPD) [4], solid solution and precipitation strengthening [5]. In addition to strengthening, the SPD technique was also reported to enhance corrosion resistance in Mg-Li–Al alloy [4]. Although SPD techniques (e.g. extrusion, rolling, equal channel angular extrusion and high pressure torsion) can impose strain as high as several hundred, the strengthening effect on bulk Mg-Li alloys is rather modest due to the saturated dislocation accumulation and/or limited plasticity of the HCP Mg-Li alloys. For instance, the highest ultimate tensile strength (UTS) of SPD-processed bulk Mg-Li alloys is reported to be 328 MPa and most of them are below 250 MPa [3,6]. Moreover, these SPD techniques are usually expensive, complex and inefficient; the maximum size of specimens produced is in the order of centimetre or even millimetre which is difficult to scale up further.

Pre-existing nano-scale twins have been reported to significantly strengthen metals while retaining considerable plasticity and work hardening, because twin boundaries (TBs) usually act as effective barriers for

CONTACT Xiang Chen xiang.chen@njust.edu.cn; Jinfeng Nie niejinfeng@njust.edu.cn; Yonghao Zhao yhzhao@njust.edu.cn

Supplemental data for this article can be accessed here. https://doi.org/10.1080/21663831.2021.1891150

dislocation motion following the empirical Hall-Petch relationship [7]. Careful literature inspection indicated that the $\{10\bar{1}2\}$ tension twins (TTW) and $\{10\bar{1}1\}$ contraction twins (CTW) are occasionally observed in the Mg-Li alloys in addition to dislocation slip. Moreover, the Mg-Li alloys can be strengthened via double twins (DTW) [8] and CTW-stacking faults (SFs) structure [9]. The SFs strengthening could be estimated as a function of the inverse of the spacing between SFs [10]. However, the above deformation twin and SFs densities are quite low and their strengthening effects are not remarkable. In addition, under high c-axis straining, deformation twinning occurring in Mg alloys was reported to inevitably introduce shear localization and stress concentration [11]. Thus, how to introduce a high density of twins and SFs into Mg-Li alloys without shear localization or stress concentration and boost their strengthening effect still remains technically challenging.

Based on Hollomon equation [12], deformation twinning and SF are susceptible to occur under high strain rate and low temperature. The strain rate of conventional SPD techniques is too low ($< 10^{-1}s^{-1}$) to introduce twins and SFs largely though they can impose a high strain of several hundred. However, rotary swaging (RS) - a widely used industrial method – can produce a deformation strain rate as high as $\sim 100\ s^{-1}$ and also a high hydrostatic stress to specimens from the die impacts. Therefore, we envisage that even low-strain RS might be beneficial for Mg alloys to introduce high density of twins and simultaneously avoid the stress concentrations in the vicinity of TBs [11]. In addition, RS also has the advantages of low cost, high efficiency and allows imposing small strain in each pass.

In this paper, so as to verify the above anticipation, Mg-4Li based alloy was first processed by the small-strain RS technique at room temperature. Mechanical properties and microstructural evolutions of swaged Mg-4Li alloy were systematically investigated, and the underlying strengthening mechanisms were finally critically appraised by the microstructure analysis.

2. Materials and methods

A coarse-grained (CG) Mg–4Li–3Al–3Zn (wt.%) rod with an initial diameter of 20.2 mm was subjected to RS at ambient temperature to a final diameter of 17.8 and 17.2 mm (i.e. a cross-area reduction of 22.4% and 27.5%; an equivalent strain of 0.25 and 0.32, respectively). Particularly, multiple passes with very low strain (~ 0.02) were carefully conducted to avoid stress concentration and shear localization.

Tensile tests were conducted at room temperature with a constant strain rate of $5\times10^{-4}\ s^{-1}$. Phase constitution was analysed by X-ray diffraction (XRD) using Cu Kα radiation operated at 40 kV and 40 mA. Scanning electron microscopy (SEM) and electron backscattering diffraction (EBSD) were employed to observe the microstructures. Transmission electron microscopy (TEM) and high-resolution TEM (HRTEM) observations were carried out to analyse types of dislocation, twin and SFs.

3. Results

3.1. Mechanical properties of swaged Mg-Li alloys

The RS working principle is schematically represented in Figure 1(a) and the picture of the as-received and RS-processed samples are shown in Figure 1(b). During swaging, four dies were evenly arranged in the circumference of the Mg-Li rod, revolved around the rod at a high speed, and at the same time made high frequency short-range strokes along the radial direction. As a result, the high strain rate and low strain of deformation from the impacting dies enhanced the micro-hardness ($\sim$75 HV for the as-received CG Mg-Li alloy) over 100 HV and finally formed a V-shaped distribution along the radial direction, as shown in Figure 1(c) and Figure S1(a,b).

Engineering stress–strain curves are shown in Figure 1(d). For the as-received sample, the UTS is 278MPa and the tensile ductility is 22%. Swaging process improved the UTS substantially to 368 MPa at the central region of the RS sample (region I) and 405 MPa at the edge region (region II), respectively, while still maintaining at least 5% tensile ductility. Figure 1(e) compares our UTS vs tensile ductility data with other literature reported values of SPD-processed multiple Mg–Li–X (X: other alloying elements) based alloys. The peak UTS of 405 MPa attained by RS far exceeds those of Mg-Li alloys reported so far. In addition, Figure 1(f) further compares our data points with the other reported UTS and ductility of Mg–Li alloys strengthened by conventional solid solution, precipitation and phase transformation [13,14]. It can be confirmed that the strength of the swaged Mg–4Li–3Al–3Zn alloy is particularly superior in the Mg-Li alloy system, albeit the small RS deformation strain of 0.32. In addition, our additional experiments indicated that an even smaller RS strain of 0.25 can enable a substantial increase of the UTS to 375 MPa (Figure S1(c)).

3.2. Microstructures of as-received and swaged Mg-Li alloys

The as-received sample consists of equi-axed CGs with an average size of about 25 μm (Figure 2(a)) and

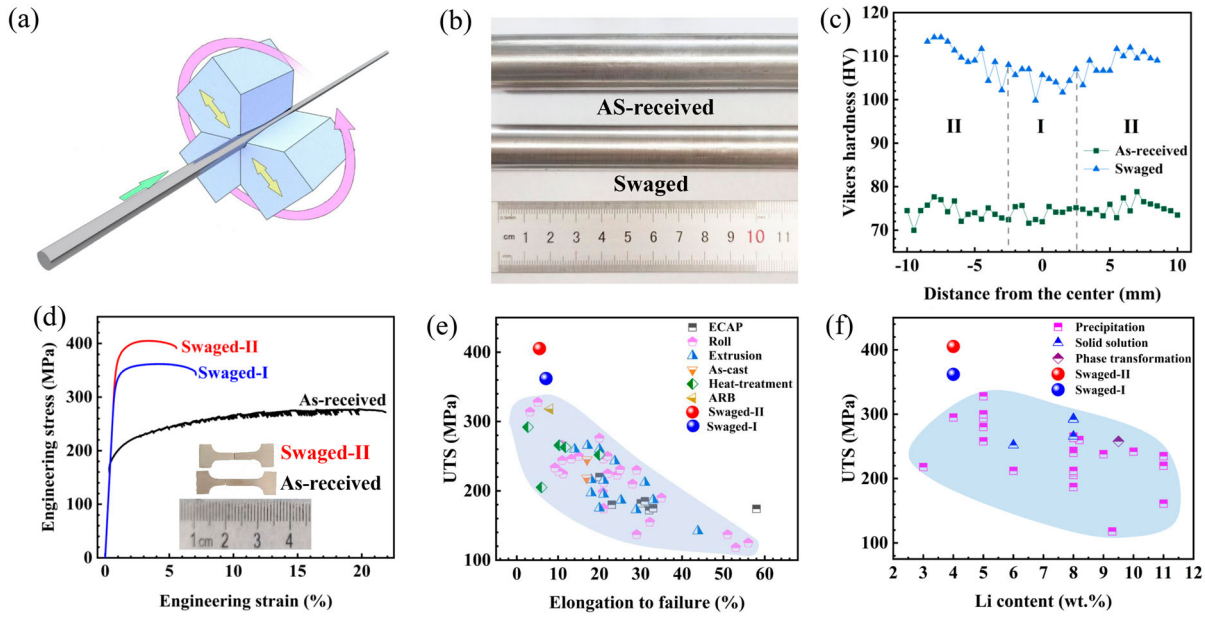

Figure 1. Mechanical properties of the swaged Mg-Li alloys. (a) Schematic illustration of the RS technique. (b) Picture of the as-received and RS-processed samples. (c) Vickers micro-hardness measured from centre to edge along the radial direction of the as-received and swaged Mg-Li alloy rods, where two regions are distinguished as I and II. (d) Typical tensile curves of the as-received and RS-processed samples. The insets are fractured tensile specimens. (e) Comparison of UTS and elongation to failure in this study with various Mg—Li—X alloys (X: alloying elements) by different SPD techniques in the literature. ECAP – equal channel angular pressing, ARB – accumulative rolling bonding. (f) The relationship diagrams between UTS and Li content of the Mg—Li—X alloys via different strengthening mechanisms [13,14].

numerous bright particles at grain boundaries (GBs). The phase constitution analysis of the Mg–4Li–3Al–3Zn alloys (Figure 2(c)) indicated that besides the indexed main phase of α-Mg, the addition of Al also leads to the formation of a small volume fraction of AlLi phase. From the energy dispersive spectrometer (EDS) measurement (Figure S2), it can be seen that the AlLi are located at the GBs.

The original grains exhibit a tendency to be slightly elongated along the direction of swaging without discernible refinement after RS processing (Figure 2(b)). It is worth noting that massive straight lamellar structures are observed in the CG interior, as pointed out by the yellow arrows, which can be further substantiated by EBSD orientation maps and corresponding mis-orientation distribution (Figure 2(d,e)). Profuse twins including DTW, CTW and TTW are discernible inside the CG matrix according to the twin-matrix orientation relationship (Figure 2(e)). Note that TTW is more pronounced. The pole figures of Figure 2(d) was plotted to elucidate the texture effect, as shown in Figure S3, as Hagihara [15] pointed out that the plastic anisotropy is an imperative factor affecting the yield stress in a BCC Mg-Li–Al single crystal sample. In our HCP Mg-Li alloy, the texture is weak with the max texture intensity is only 7.78 which can be well explained by the low deformation strain of RS. Moreover, the deformation did not cause any new phase transformation (Figure 2(c)).

To reveal the main reason for the remarkable strength elevation, the microstructure of the swaged sample from the longitudinal edge section (region II with UTS of 405 MPa) was investigated by TEM and HRTEM close to the $[11\bar{2}0]$ zone axis. As shown in the TEM images in Figure 3(a) and Figure S4, plenty of twins and dislocations are introduced into the RS-processed sample. The frequently observed TBs in the swaged sample are marked by the orange arrows in Figure 3(a). Moreover, there is a high density of line contrast within a narrow deformation twin, presumably the SFs as revealed below. Careful examination of the dislocation structure taken along the direction of $[11\bar{2}0]$ shows that the majority of dislocation arrays in the twin has a strong tendency to align with the basal plane (Figure 3(b)), which are identified as basal $<a>$ type dislocations. This is due to the fact that the resolved shear stress (CRSS) of basal slip is much lower than that of non-basal slip.

Based on the $g \cdot b = 0$ invisible criterion, $<c>$ dislocations with a Burgers vector $b = <0001>$ are mostly able to be observed if the two beam condition is set as $g = 0002$, and the $<a>$ dislocations with $b = 1/3<11\bar{2}0>$ are visible in the condition of $g = 0\bar{1}10$. Accordingly, all the visible dislocation

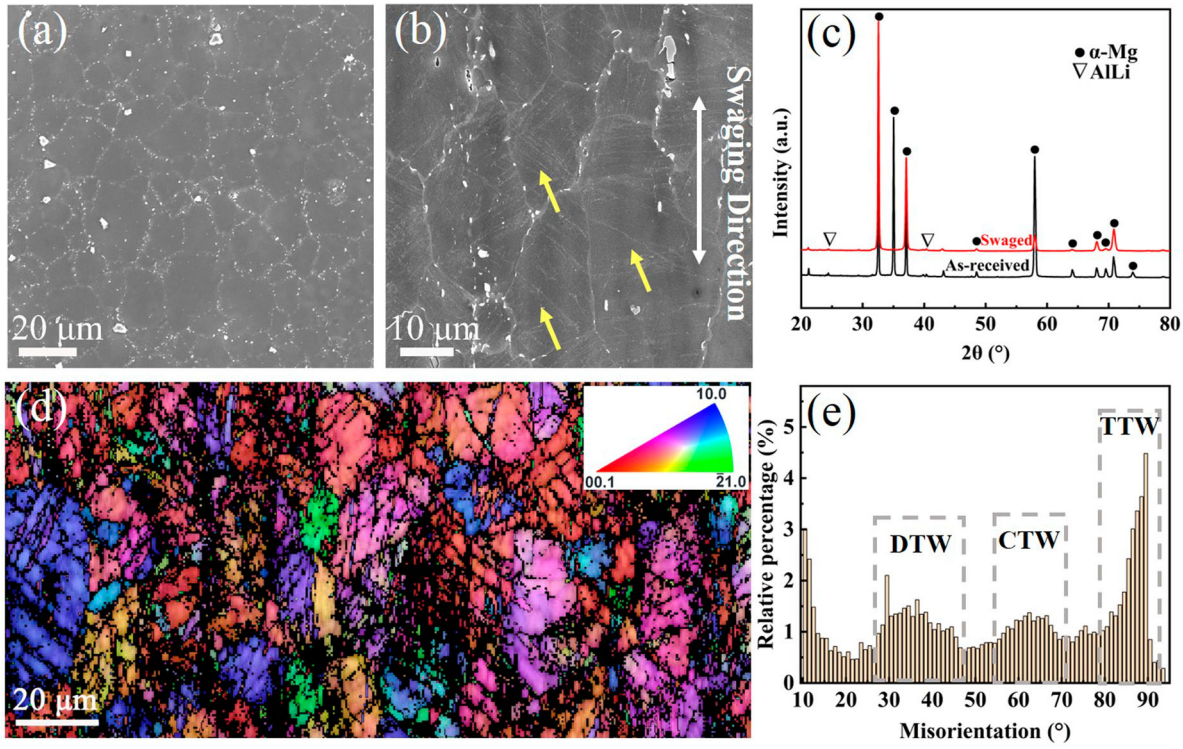

Figure 2. Morphology, phase constitution and orientation mapping of the as-received and swaged Mg-Li alloys. (a,b) Typical SEM images of the (a) as-received and (b) RS-processed Mg-Li samples; The yellow arrows in (b) indicate the newly formed lamellar structures. (c) Corresponding XRD characterization showing the phase constitution. (d) EBSD orientation mapping for the RS-processed Mg-Li sample. The inset is colour code in which red, green and blue indicate grains having $< 00.1 >$, $< -21.0 >$ and $< 10.0 >$ directions, respectively. (e) Corresponding mis-orientation distributions of the RS-processed sample. The $\{10\bar{1}1\} - \{10\bar{1}2\}$ double twins, $\{10\bar{1}1\}$ contraction twins and $\{10\bar{1}2\}$ tension twins are marked as DTW, CTW and TTW, respectively.

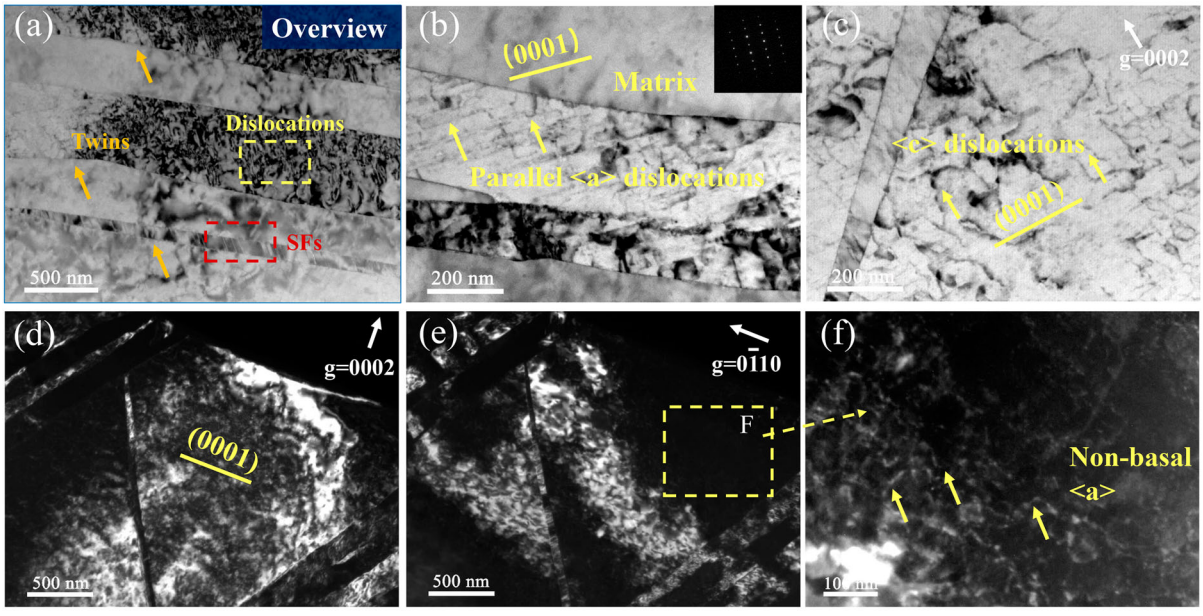

Figure 3. Dislocation activities in the Mg-Li alloys by RS. (a,b) TEM photographs of typical deformation microstructures taken from the longitudinal edge section near the $[11\bar{2}0]$ zone axis. The inset shows the SAED pattern. (c – f) Bright and dark field TEM images in two-beam conditions using different diffraction vectors near the $[11\bar{2}0]$ zone axis. (c,d) under g = 0002. (e) under g = $0\bar{1}10$. (f) An enlarged image of selected area in (e). The yellow straight lines in (c) and (d) highlight the trace of (0001) basal plane.

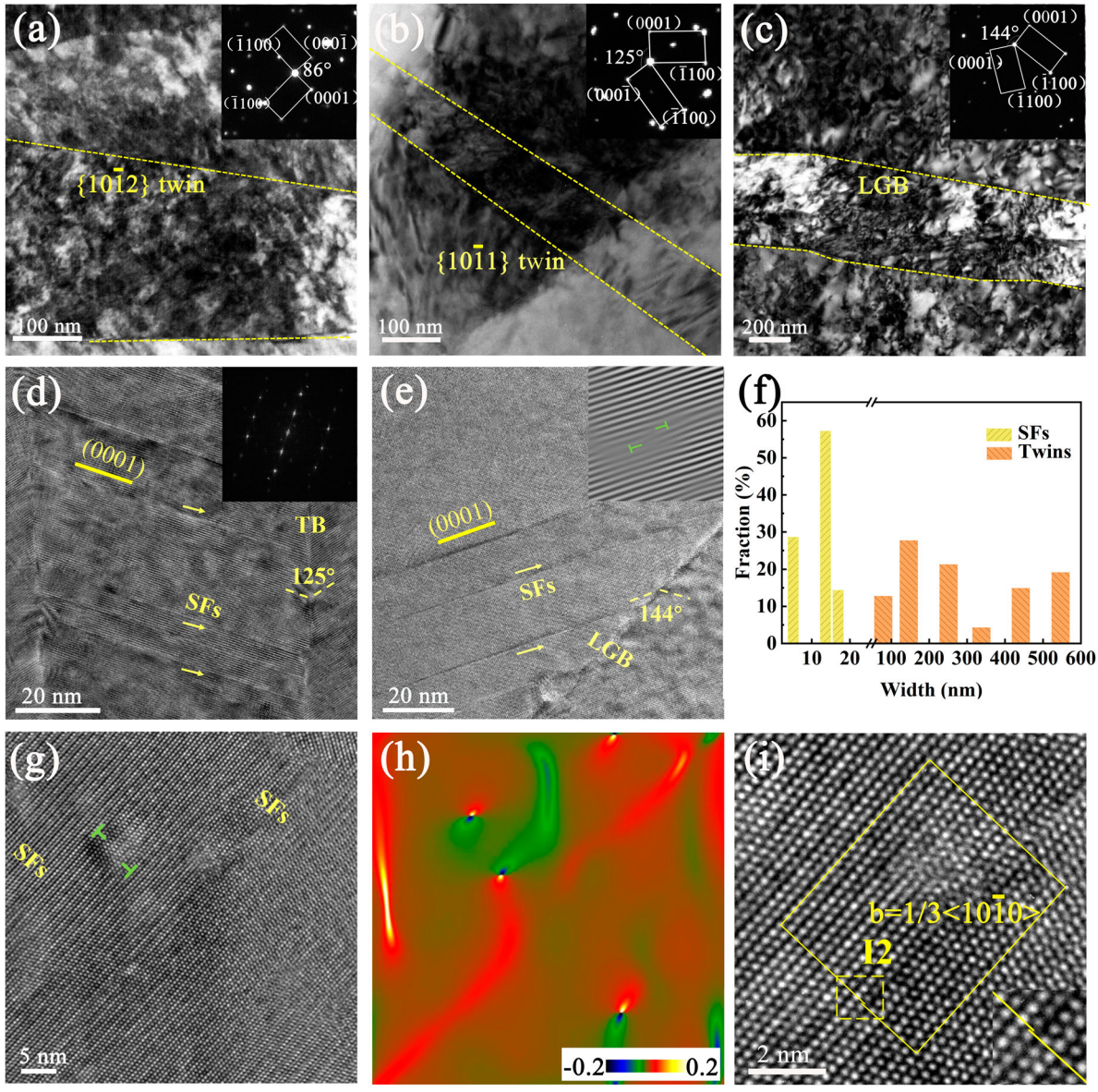

Figure 4. Illustration of twinning and SFs strengthening mechanisms revealed by (HR)TEM. (a – c) Low magnified TEM images and corresponding SAED patterns of lamellae structures in the RS-processed Mg-Li alloy. (d) HRTEM image and corresponding FFT showing SFs in a {10$\bar{1}$1} twin. (e) HRTEM image and corresponding inverse Fast-Fourier transform (IFFT) image of SFs in a lamellar grain; (f) The variation of width for twins and SFs; (g,h) Atomic-scale TEM images of SFs and corresponding GPA analysis. (i) HRTEM image showing an I2 fault bounded by 1/3 $<\{10\bar{1}1\}>$ Shockley partials.

segments (yellow arrows in Figure 3(c)) observed in the condition of g = 0002 are $<c>$ dislocations. Recent experiments have demonstrated that a $<c+a>$ full dislocation can dissociate into a $<c>$ and an $<a>$ dislocation at room temperature [16]. Thus, it is reasonable to assume that most of observed non-basal $<c>$ dislocations can be interpreted by the dissociation of pyramidal $<c+a>$ dislocations (Figure 3(c)). The two-beam dark field images using g = 0002 and g = 0$\bar{1}$10 near the direction of [11$\bar{2}$0] zone axis reveal more dislocations in this area (see Figure 3(d,e)). As shown in Figure 3(d), no dislocation lines are seen inside the grain when g = 0002 indicating there are no $<c>$ or $<c+a>$ in this grain. However, different from basal $<a>$ dislocations shown in Figure 3(b), numerous non-basal $<a>$ dislocations can be seen in the same image area with g = 0$\bar{1}$10 combined with an analysis of slip plane traces (Figure 3(e,f)). The enlarged image in Figure 3(f) shows that these visible non-basal $<a>$ type dislocations are distributed randomly as depicted by the yellow arrows.

Figure 4(a)–(c) present the bright-field TEM images of deformation twins inside the swaged samples and the corresponding selected area electron diffraction (SAED)

patterns near the [11$\bar{2}$0] zone axis. The dashed yellow lines indicate approximate locations of the twins. The twins are determined to be {10$\bar{1}$2} TTWs and {10$\bar{1}$1} CTWs according to the SAEDs with the angles between the twin 0001 planes and the matrix 0001 planes being 86° and 125°, respectively (Insert in Figure 4(a,b)). As shown in Figure 4(c), another kind of lamellar structure has a unique mis-orientation angle of 144° relative to the traditional twins. Previous studies defined it as a special lamellar GB (LGB) formed by multiple twinning, where neighbouring grains shared the same [11$\bar{2}$0] zone axis [17]. At the early stage of RS, large numbers of the primary twins were nucleated from GBs in parallel, forming long and narrow twins (see Figure 3(d)). With further straining, localized stresses were generated at twin tips and such stress localization catalysed nucleation of new twins in some primary twins. Thus, the grain re-oriented again due to the secondary twinning which may explain the formation of LGBs widely observed in the swaged samples with unique mis-orientation angle.

As shown in Figure 4(d), a high density of parallel SFs are observed to lie on the basal plane inside a {10$\bar{1}$1} twin. The streak reflections in the fast Fourier transform (FFT) pattern (Insert in Figure 4(d)) are a sign hinting to basal-plane SFs. Further, some SF segments are also well aligned linked to the LGB in Figure 4(e) and an array of misfit dislocations is identified from the corresponding inverse Fast-Fourier transform (IFFT) image. As clearly shown in the insert IFFT image, the core of this misfit dislocation is located at the end of the extra half plane, suggests that these basal SFs belong to the I1 type. Meanwhile, SFs can also be observed in {10$\bar{1}$2} TTWs (see Figure S5). The statistic result in Figure 4(f) reveals that the average spacing values of twins and SFs in the swaged sample are 289 and 11 nm, respectively.

To probe the dislocation interactions with SFs, the atomic-scale structure of SFs was clarified by aberration-corrected TEM (Figure 4(g)−(i)). First, the local displacement variations along SFs, which can reflect the strain distribution, are delineated by geometric phase analysis (GPA) of the HRTEM image (Figure 4(h)). Quantitative GPA measurement shows that the largest dilatation (light-red colour) region is associated with the misfit dislocation. The determined position of dislocation cores from this map is consistent with that in Figure 4(g). The maximum values of strain nearby the interface of SFs indicates SFs on basal planes are expected to provide similar effect as reported for deformation twins on impeding dislocation movement. An enlarged HRTEM in Figure 4(g) were used to identify the accurate types of SFs and their bounding dislocations (Figure 4(i)). The partial dislocations forming SFs were determined by drawing Burgers circuits around the dislocation cores. It is seen that the closure failure of the Burgers circuit indicates an I2 stacking sequence formed by 1/3 $<10\bar{1}0>$ partial dislocation.

The only one literature about RS of Mg-Al-Zn alloy mainly focuses on inducing pronounced grain refinement via high strain (up to 2.77) and thus overlooks the small strain regime [18]. As expected, a small-strain RS can avoid the stress concentrations and cracks in the vicinity of TBs. Regarding the formation mechanisms of observed I1 and I2 faults, a thin three-layer and four-layer of face-centre cubic (FCC) stacking structure are introduced into the HCP α-Mg matrix, respectively (see Figure 4), which remain glissile on basal planes to accommodate the basal strain and change the stacking sequence[19]. The basal plane SFs were expected to sustain a certain amount of the swaging strain, which is substantiated by the GPA strain analysis (see Figure 4 and Figure S6).

4. Discussions

Our current results demonstrate that a small-strain RS processing brings about a high UTS in a CG Mg-4Li based alloy without changing chemical composition or phase constitution. The enhanced mechanical strength is intimately related to the high density of deformation twins, SFs and dislocations formed in the CG interior, as the GB and precipitation strengthening is negligible. Our RS introduced more different types of twins and SFs as well as higher densities than those reported in the literature [9,20] due to the constant change of loading shear stress direction and high strain rate facilitates the activation of multiple twinning and SFs. Deformation twinning in Mg alloys is generally activated at lower strains, which is one of the main sources of work hardening during the early stages of plastic deformation. The tangled dislocations observed in the interior of twins demonstrates the effective role of TBs in prohibiting dislocation movement (Figure 3(a)). As discussed above, SFs may also play a distinctive role in dislocation gliding and dislocation cross-slip during the plastic deformation process, hence exerting significant impacts on mechanical properties [16]. When the dislocations encountered the SFs, they could either (1) cut or interact with SFs in order to sustain plastic deformation or (2) accumulate nearby the SFs and accommodate strain hardening. It was previously suggested that the yield strength follows a linear relationship with the reciprocal of average spacing of SFs in the Mg alloys. Accordingly, the strengthening contributions from twins and SFs can be calculated by the following

equation [21]:

$$\Delta\sigma = m(k_1\lambda^{(-1/2)} + k_2 d^{-1}) \quad (1)$$

where λ and d are the average widths of twins and SFs, respectively; m is the volume fraction, k_1 is the Hall-Petch constant (0.35 MPa $m^{1/2}$), k_2 is the experimental constant (3780 MPa nm). Taking m as 0.135 (measured statistically from Figure 2(b)), the estimated strength from twins is about 88 MPa and the strength contributed by SFs is about 46 MPa. The increased yield strength is approx. 188 MPa determined from the tensile tests. Hence, the introduction of twins and SFs enables the yield strength elevation by 71%. This strongly supports that the presence of nano-spaced twins and SFs during swaging treatment is the main strengthening contribution to the observed ultrahigh strength. For better illustration, the strengthening mechanisms in the swaging process is summarized in Figure S7. Nano-spaced twins and SFs provide a possibility to attain a higher fraction of coherent interfaces which can act as dislocation sinks and are effective in obstructing dislocation motion. This work sheds key insights into the untapped potential in attaining light, strong and applicable Mg–Li alloys by exploring a low-cost and facile technique.

5. Conclusion

In summary, a high strength was successfully achieved in a CG HCP Mg–Li alloy by means of an industrial method of RS technique at room temperature. Interestingly, a low-strain swaging process triggers massive twins and SFs in the grain interior which are effective in impeding the movement of dislocations and retaining strain hardening. Taking into account the low-cost and facile process, we expect that the industrial utilization of bulk ultra-light Mg-Li alloys with unprecedented strength will be greatly accelerated.

Acknowledgements

Y.H. Zhao and X. Chen acknowledge scientific & technical assistance from Jiangsu Key Laboratory of Advanced Nanomaterials and Technologies, Nanjing University of Science and Technology.

Disclosure statement

No potential conflict of interest was reported by the author(s).

Funding

This work is supported by the National Key R&D Program of China [grant number 2017YFA0204403), National Natural Science Foundation of China [grant numbers 51971112, 51731007, 52001165 and 51931003], Natural Science Foundation of Jiangsu Province, China [grant number BK20200475], and the Fundamental Research Funds for the Central Universities [grant numbers 30919011405 and 30920021160].

ORCID

Xiang Chen http://orcid.org/0000-0002-4802-9684
Qingzhong Mao http://orcid.org/0000-0001-7527-4266

References

[1] Knochel P. A flash of magnesium. Nat Chem 2009;1: 740–740.
[2] Zhang C, et al. Electrochemical characterization of the corrosion of a Mg–Li alloy. Mater. Lett. 2008; 6 2:2177–2180.
[3] Liu Y, et al. Study on the Mg-Li-Zn ternary alloy system with improved mechanical properties, good degradation performance and different responses to cells. Acta Biomater. 2017;62:418–433.
[4] Mineta T, Sato H. Simultaneously improved mechanical properties and corrosion resistance of Mg-Li-Al alloy produced by severe plastic deformation. Mater Sci Eng A. 2018;735:418–422
[5] Tang S, et al. Precipitation strengthening in an ultralight magnesium alloy. Nat. Commun.2019;10:1003.
[6] Cao F, et al. Superplasticity of a dual-phase-dominated Mg-Li-Al-Zn-Sr alloy processed by multidirectional forging and rolling. Mater. Sci. Eng. A. 2017;704:360–374.
[7] Lu L, et al. Revealing the maximum strength in nanotwinned copper. Science.2009;323:607–610.
[8] Fu H, et al. Achieving high strength and ductility in magnesium alloys via densely hierarchical double contraction nanotwins. Nano Lett. 2017;17:6117–6124.
[9] Peng Q, et al. Nanoscale coherent interface strengthening of Mg alloys. Nanoscale.2018;10:18028–18035.
[10] Jian WW, et al. Physics and model of strengthening by parallel stacking faults. Appl. Phys. Lett. 2013;103:133108.
[11] Barnett MR. Twinning and the ductility of magnesium alloys: part II. "contraction" twins. Mater. Sci. Eng.A.2007;464:8–16.
[12] Li YS, et al. Effect of the zener–Hollomon parameter on the microstructures and mechanical properties of Cu subjected to plastic deformation. Acta Mater.2009;57:761–772.
[13] Xu DK, et al. Effect of icosahedral phase on the crystallographic texture and mechanical anisotropy of duplex structured Mg–Li alloys. Mater.Des.2015;88:88–97.
[14] Zhao J, et al. Influence of heat treatment on microstructure and mechanical properties of as-cast Mg–8 Li–3 Al–2 Zn–xY alloy with duplex structure. Mater Sci Eng A. 2016;669:87–94.
[15] Hagihara K, et al. Enhancement of plastic anisotropy and drastic increase in yield stress of Mg-Li single crystals by Al-addition followed by quenching. Scr. Mater.2019;172:93–97.
[16] Wu Z, et al. Mechanistic origin and prediction of enhanced ductility in magnesium alloys. Science. 2018; 359:447–452.
[17] Zhou H, et al. Effect of Ag on interfacial segregation in Mg–Gd–Y–(Ag)–Zr alloy. Acta Mater.2015;95:20–29.

[18] Estrin Y, et al. Effect of rotary swaging on microstructure, texture, and mechanical properties of a Mg-Al-Zn alloy. Adv. Eng. Mater.2020;22:1900506.
[19] He C, et al. Unexpected partial dislocations within stacking faults in a cold deformed Mg—Bi alloy. Acta Mater.2020;188:328–343.
[20] Xiang Q, et al. Effect of rolling-induced microstructure on corrosion behaviour of an as-extruded Mg-5 Li-1 Al alloy sheet. corros. Science.2017;119:14–22.
[21] Peng Q, et al. Interactive contraction nanotwins-stacking faults strengthening mechanism of Mg alloys. Acta Mater.2019;169:36–44.